Chemical Engineering Journal 509 (2025) 161119

Contents lists available at ScienceDirect

Chemical Engineering Journal

journal homepage: www.elsevier.com/locate/cej

Robust and efficient electroreduction of CO_2 to CO in a modified zero-gap electrochemical cell

Siyu Zhong [a,*], Pengfei Sui [b], Peter Holtappels [a], Alexander Navarrete [a], Fengwang Li [c], Roland Dittmeyer [a,*]

[a] Institute for Micro Process Engineering (IMVT), Karlsruhe Institute of Technology (KIT), Hermann-von-Helmholtz-Platz 1, 76344 Eggenstein-Leopoldshafen, Germany
[b] Department of Chemical and Materials Engineering, University of Alberta, 9211 116 Street NW, Edmonton, Alberta T6G 1H9, Canada
[c] School of Chemical and Biomolecular Engineering and ARC Centre of Excellence for Green Electrochemical Transformation of Carbon Dioxide, University of Sydney, Sydney, NSW, Australia

ARTICLE INFO

Keywords:
CO_2RR
Zero-gap electrolyzer
Energy efficiency
Faradaic efficiency
Operation stability

ABSTRACT

Excellent energy efficiency and system stability are critical factors guiding the practical application of carbon dioxide reduction reaction (CO_2RR) systems. This work promotes reduction reaction kinetics in a modified zero-gap electrolyzer by regulating the operation temperature and pressure. The energy efficiency of the CO_2RR system is enhanced, such as 52.6 % at a current of 1.2 A under alkaline conditions and 49.4 % under neutral conditions, with the characteristics of low voltage and high Faradaic efficiency. In addition, the optimization of the reaction microenvironment effectively alleviates the precipitation issue, enabling the system to operate stably for more than 100 h, with a Faradaic efficiency of more than 90 % for CO generation. Engineering-integrated electrochemistry inspires the future development of CO_2RR technology.

1. Introduction

The electrochemical reduction of carbon dioxide powered by renewable sources such as solar or wind energy, stands out as a promising technology for facilitating the sustainable energy transition [1,2]. The primary product carbon monoxide (CO) from CO_2RR is a versatile and fundamental industrial feedstock utilized in the synthesis of a wide range of chemicals. It constitutes a main component of syngas, which can be further converted into methanol, olefins, and even sustainable aviation fuels [3–5]. However, the development of CO_2RR technologies is currently constrained by high energy consumption, while stability and energy efficiency are the key indicators for evaluating the scalability and economic feasibility [6,7]. Although efficient catalysts are the decisive factor in improving the selectivity of specific products [8–10], the overall energy efficiency and operational performance of the electrochemical reaction are also influenced by the reactor configuration [11–13].

The zero-gap electrolyzer configuration featuring adjacent electrodes, in which the catholyte is omitted, is aimed to minimize ohmic resistance and activate the catalytic reactions with a low overpotential [14–16]. This setup also permits direct contact between the catalyst and the ion exchange membrane, which not only significantly improves mass transport dynamics but also preserves the structural integrity of the electrodes [17–19]. Alkaline and neutral media are used to suppress the competitive hydrogen evolution reaction (HER) and strengthen the selectivity of CO_2RR. Although there is no liquid electrolyte flowing through the cathode in the zero-gap electrolyzer, vapor carried by the humidified CO_2 stream and water transported from the anode through the membrane are reactants for the reduction reaction ($CO_2 + H_2O + 2e^- \rightarrow CO + 2OH^-$) [20,21]. However, the reaction between OH^- and CO_2 on the cathode surface leads to the formation and precipitation of carbonates, particularly at high current densities [22,23]. Engineering approaches are introduced as strategies to address these issues, such as increasing the reaction temperature and pressure [24], which kinetically favors the reduction process to improve energy efficiency, and maintaining a stable microenvironment at the cathode to extend the system lifetime.

This work investigated the operational parameters of an electroreduction system based on a zero-gap electrolyzer, and the management of the cathode microenvironment to boost the energy efficiency for CO_2-to-CO and to prolong system longevity. With employing commercially available silver catalysts, the modified zero-gap electrolyzer

* Corresponding authors.
E-mail addresses: siyu.zhong@kit.edu (S. Zhong), roland.dittmeyer@kit.edu (R. Dittmeyer).

https://doi.org/10.1016/j.cej.2025.161119
Received 31 October 2024; Received in revised form 31 January 2025; Accepted 27 February 2025
Available online 28 February 2025

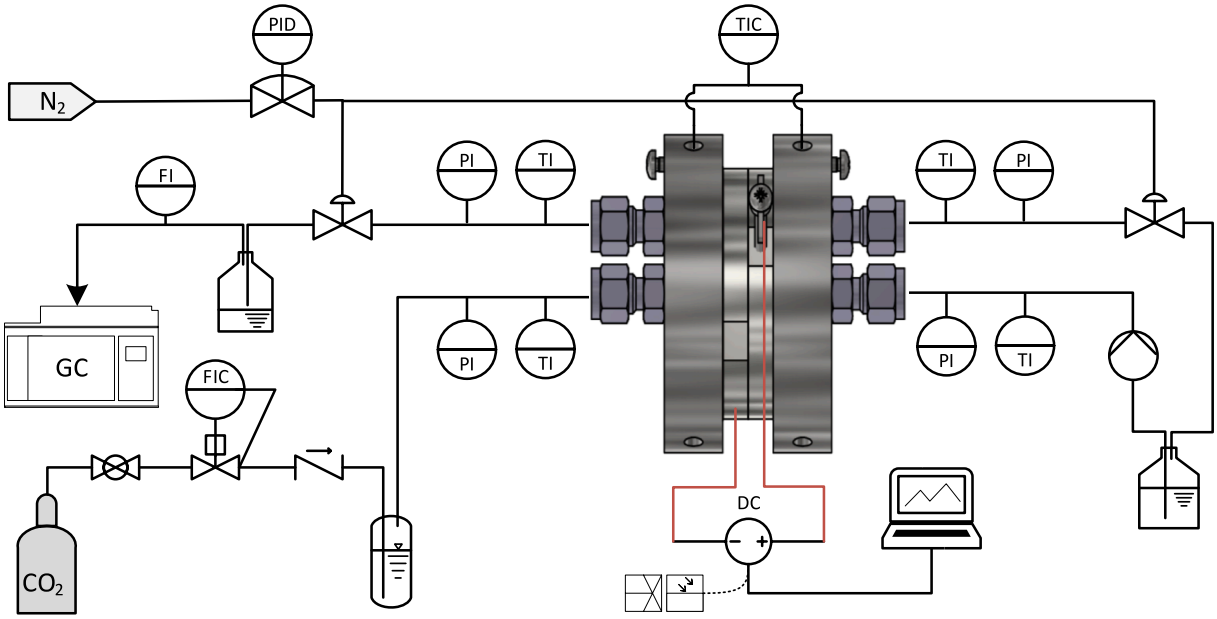

Fig. 1. PID of electrocatalytic reduction of CO_2 system with a zero-gap electrolyzer.

demonstrated a current of up to 4.2 A with a cell voltage below 4 V at ambient temperature, and indicated the downward trend of electricity costs as the operating temperature rose. It further exhibited a high energy efficiency of over 50 % at a current density of 100 mA/cm^2 under heated or pressurized conditions. Additionally, the device enabled stable operation for over 100 h at a total current of 1.2 A, with a CO Faradaic efficiency of no less than 90 %. This research provides fundamental insights for electrochemical CO_2 reduction technologies in future applications.

2. Experimental section

2.1. Electrolyzer and test bench modification

The zero-gap reactor was adapted from a commercial electrolyzer (Parr Instruments). Here, two titanium flow field plates were refabricated, featuring spiral channels with a width of 0.75 mm, a depth of 0.65 mm, and a pitch of 1.3 mm. Titanium bolts, inserted and tightened from the side of the flow field plate, here functioned as current collectors. The membrane electrode assembly (MEA) and flow plates were sandwiched between two stainless steel plates with a diameter of 9 cm and fastened by eight bolts, with polyimide foils as insulation between each layer. Liquid and gas feeds flowed through the housings to the anode and cathode, respectively.

The process and instrument diagram (PID) of the proposed CO_2 electroreduction system based on a zero-gap electrolyzer is shown in Fig. 1 and the photos of devices are shown in Fig. S1. A flow indicator controller (FIC) and a high-performance liquid chromatography (HPLC) pump are employed to maintain precise and stable flow rates for both gas reactant and anolyte. Two cartridge heaters are installed on each stainless steel plate, close to plug-in electronic temperature sensors, whose temperature is precisely regulated by an integrated temperature indicator controller (TIC) to ensure a stable and uniform thermal environment inside the electrolyzer. The back pressure regulators and electronic pressure indicator controller (PIC) work together to dynamically adjust and stabilize the consistent pressure at the cathode and anode sides. In addition, multiple electronic pressure indicators (PI) and temperature indicators (TI) are strategically distributed throughout the system to monitor temperature sensitively. The resultant gaseous products are analyzed in real time by a gas chromatograph (GC), enabling detailed component characterization.

2.2. Preparation of MEA

The electrodes were prepared by spraying the catalyst ink on the gas diffusion layers. Silver nanopowder (APS 20–40 nm, 99.9 %, Thermo Scientific Chemicals) and iridium oxide nanopowder (Fuel Cell Store) were selected as catalysts. Carbon paper (Sigracet 39 BB) and platinized titanium fiber felt (Fuel Cell Store) served as cathode gas diffusion layers (cGDL) and anode gas diffusion layers (aGDL), respectively. For the cathode, the catalyst ink was prepared by ultrasonically mixing 5 wt% of Nafion solution (40 μL) and Ag nanopowder (30 mg) in isopropyl alcohol (2 mL) for 20 min. Then the ink was manually sprayed onto the carbon paper placed on a heated plate at 80 °C, and the mass loading of the cathode catalyst layer (cCL) was approximately 1.5 ~ 2.0 mg/cm^2. The same preparation procedure method was employed to coat IrO_2 on platinized titanium fiber felt as the anode catalyst layer (aCL). The area of both electrodes was 12 cm^2.

2.3. Characterizations

Surface characterization of the samples was carried out using a Zeiss Gemini SEM 500 microscope with a thermal Schottky field emission cathode, and the elemental distribution mappings were obtained using an Oxford energy dispersive X-ray spectrometer (EDS) instrument with a silicon drift detector. The cross-sectional images of the coated samples were collected from scanning electron microscopy (SEM) (JXA 8530F, JEOL) with various magnifications, and the catalyst distribution in the coating layer was analyzed with wavelength-dispersive X-ray spectroscopy (WDX). The contact angle measurements with 5 μL droplets of deionized water were conducted using a DSA25S Drop Shape Analyzer for photography and angle calculation.

2.4. Electrocatalytic performance

All electrochemical CO_2 reduction tests were recorded on a Biologic VSP-300 potentiostat with a 10-ampere current booster. Anion exchange membranes (Sustainion X37-50 Grade RT) were activated in 1 M KOH for 24 h, in 0.1 M $KHCO_3$ for 12 h, and rinsed with ultrapure water before use. In the modeled zero-gap MEA electrolyzer described above, the cell voltage was the potential difference between the cathode and the anode with no iR compensation. The aqueous anolyte was circulated by an HPLC pump at a flow rate of 30 mL/min. CO_2 was bubbled through a

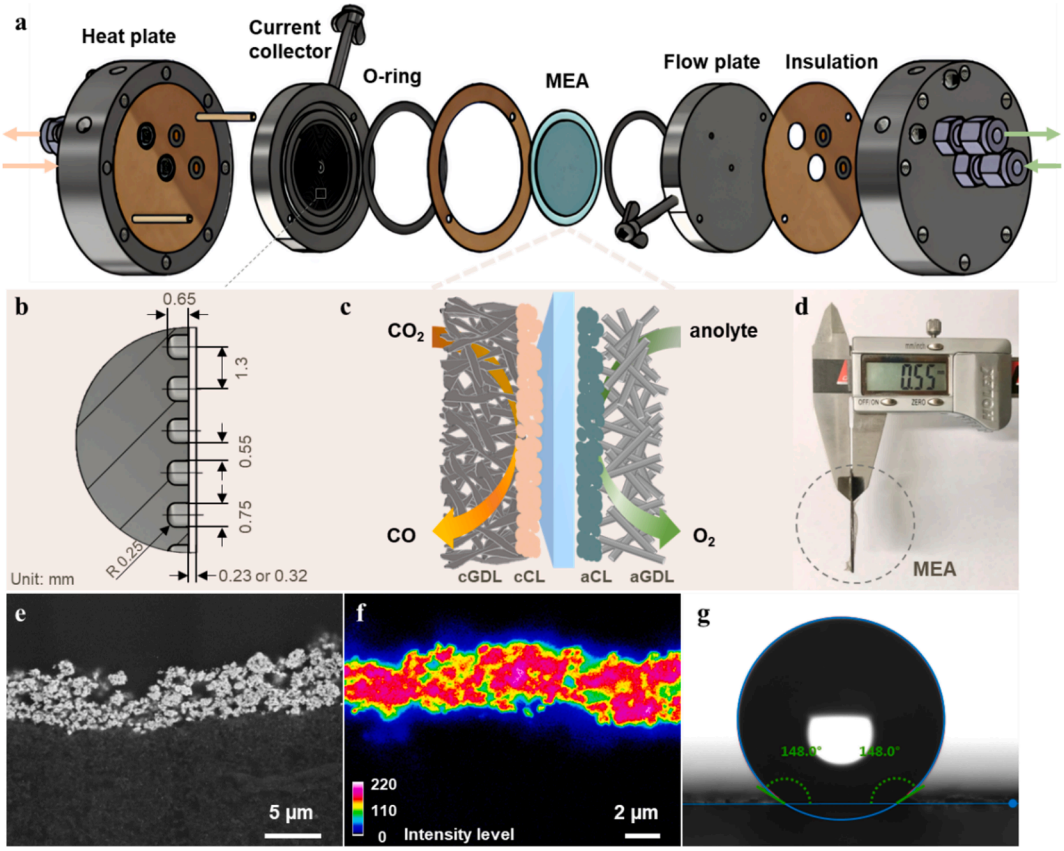

Fig. 2. (a) Schematic diagram of the modified zero-gap electrolyzer. (b) Fabrication specifications for flow field plates with microchannels. (c) Cross-section schematic of the MEA, including the catalyst layers, GDLs, and an ion exchange membrane. (d) Photograph showing the thickness of the prepared MEA. (e) Cross-sectional SEM images and (f) intensity distribution of airbrushed Ag catalyst on carbon GDL. (g) Photograph of contact angle measurement on the fresh Ag@C electrode.

cylinder filled with water at 50 °C before entering the reactor, and the CO_2 was fed for 10 min before each electrolysis experiment to remove residual air. The flow rate of the CO_2 gas into the cathode was kept at 90 standard cubic centimeters per minute (sccm) by a mass flow controller (SLA5800 Series, Brooks) and another float-type flowmeter as an outlet reference. Each assembled MEA was activated in the voltage range of 0.5–4.0 V by three linear sweep voltammetry (LSV) tests. Electrochemical impedance spectroscopy (EIS) measurements were performed at several currents with a voltage amplitude of 5 mV, and the frequency limits were set from 100 kHz to 1 Hz.

2.5. Product quantification

The composition of the output gas was analyzed by a gas chromatograph (SHIMADZU 2010 plus) with a packed HP-PLOT Q column. Ultra-high purity Ar gas (99.9999 %) was used as the make-up gas. A flame ionization detector (FID) for C1-C3 quantification and a thermal conductivity detector (TCD) for H_2 quantification were installed in the gas chromatograph. The signal response of the TCD and FID was calibrated by a range of commercial standard gases previously. The GC was set to automatically draw samples every 12 min and at least three consecutive detection data were collected to calculate the Faradaic efficiency and error bars at each tested current density. The Faradaic efficiency (FE) of products was calculated by the equation:

$$FE = \frac{Q_i}{Q_{total}} \times 100\ \% = \frac{n \times v \times x \times \frac{F}{RT}}{I} \times 100\ \%$$

where Q_i is the electrons stored in the products and Q_{total} stands for the total charge consumption, n is the number of transferred electrons, v is the flow rate of CO_2 gas, x is the volume fraction of product determined by gas chromatograph, F is the Faradaic constant, p is the pressure, T is the room temperature and R is the ideal gas constant with a value of 8.314 J mol/K, and I is the recorded total current [25]. The energy efficiency (EE) calculations based on the thermoneutral potential (change in reaction enthalpy) directly reflect the efficiency relative to the chemical energy stored in the final product [26]. The enthalpy change (ΔH) of the overall reaction of $CO_2 \rightarrow CO + ½O_2$ is 283 kJ/mol, which gives a thermoneutral potential E^n of 1.47 V [27,28], and the energy efficiency of the system is given by the equations:

$$E^n = \frac{\Delta H}{nF}$$

$$EE = \frac{E^n}{E_{(i)}} \times FE$$

where n is the number of transferred electrons, F is the Faraday constant, $E_{(i)}$ is the recorded cell voltage of the zero-gap electrolyzer and FE is the Faradaic efficiency of CO at a given current.

3. Results and discussion

3.1. Characterization of MEA

The modified zero-gap reactor includes a core membrane electrode assembly with the flow fields and housings on both sides, as illustrated in Fig. 2a. In the headspace over the flow channels (facing the ion exchange membrane), a gap of 320 μm was reserved for the cathode electrode, while another one was 230 μm for the anode, as shown in

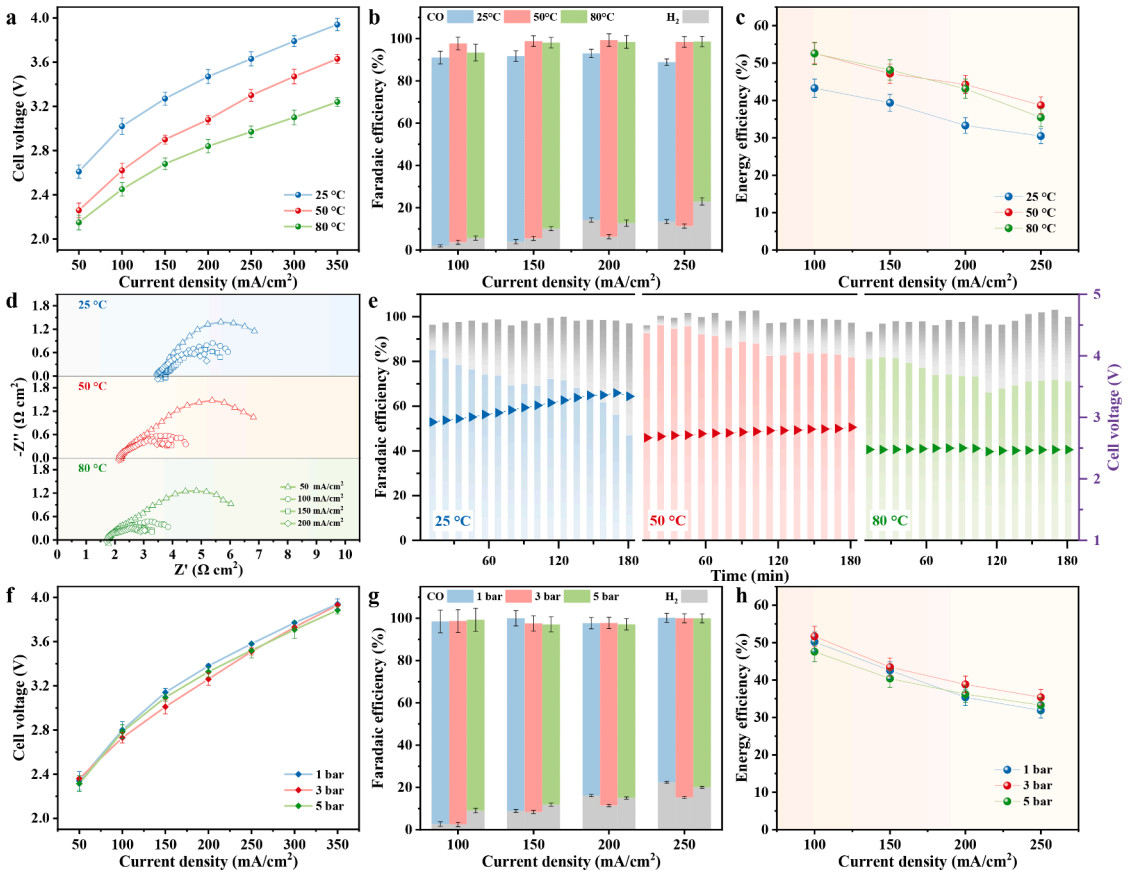

Fig. 3. CO_2RR performance with 1 M KOH anolyte in the modified zero-gap electrolyzer. (a) Polarization curves, (b) Faradaic efficiencies of CO and H_2, (c) the calculated energy efficiency, and (d) Nyquist plots at each current density under operating temperatures of 25 °C, 50 °C, and 80 °C. (e) The recorded cell voltages and corresponding FE_{CO} at a current of 1.2 A during 3 h of operation under operating temperatures of 25 °C, 50 °C, and 80 °C. (f) Polarization curves, (g) Faradaic efficiency, and (h) energy efficiency at each current density under a pressure of 1 bar, 3 bar, and 5 bar.

Fig. 2b. An anion exchange membrane (AEM) with a thickness of 50 μm was placed between the electrodes, as Fig. 2c shows, to fulfill the MEA. To yield a compact design of the modified electrolyzer, the entire MEA including GDLs, catalyst layers, and ion exchange membrane, was compressed between the two flow field plates, maintaining a total thickness of 550 μm (Fig. 2d). Commercial silver nanoparticle catalysts with a primary diameter of approximately 50–100 nm can be distinguished from the SEM image in Fig. S2, and the top view SEM of the cathode electrode reveals that the Ag catalyst is uniformly coated on the carbon GDL. The crystal structure and phase purity of the catalysts were examined by XRD in Fig. S3; the characteristic peaks at 38.1°, 44.3°, 64.4°, and 77.4° were assigned to the diffraction of (1 1 1), (2 0 0), (2 2 0), and (3 1 1) crystal planes for Ag (JCPDS No. 04-0783), respectively [29,30]. The thickness of the spray-coated Ag catalyst layer on GDL is about 5 μm without obvious catalyst agglomeration, as shown from the cross-sectional SEM image (Fig. 2e), where the spray of ink mist and rapid solvent evaporation expedited the formation of a clear and uniform catalyst layer on the GDL. Moreover, the intensity distribution spectrum in Fig. 2f demonstrates that Ag nanoparticles are well distributed in the direction perpendicular to the GDL. A catalyst layer of appropriate thickness provides numerous electrochemically active sites essential for CO_2RR and avoids the electrical contact between the membrane and the bare carbon GDL [31,32]. The catalyst side of the fresh Ag/C electrode initially exhibits a water contact angle of 148° (Fig. 2g), and its hydrophobicity can ensure rapid gas diffusion and establish an effective reaction interface in the cathode [33,34]. The SEM micrographs in Fig. S4 show that the catalyst IrO_2 powder with nanoparticle size is air sprayed onto the surface of the titanium fiber to form the IrO_2@Ti anode. The catalyst side of the fresh IrO_2@Ti electrode initially shows a water contact angle of 136.3° (Fig. S5), which allows smooth penetration of the anolyte and rapid diffusion of the produced oxygen through the open structure.

3.2. Notable energy efficiency in alkaline anolyte

The no-catholyte MEA system with 1 M KOH flowing anolyte exhibits a high reaction rate with a current of 4.5 A at a cell voltage of 4 V under ambient temperature conditions, as indicated by the LSV curves in Fig. S6. This is further exemplified by a large current of 7 A at the same cell voltage when the operating temperature is increased to 80 °C. The maximum operating temperature of the membrane should not exceed 90 °C to prevent decreased proton mobility through the membrane and flooding caused by increased water crossover [35,36]. Fig. 3a shows the impact of three representative operating temperatures on cell voltage at various current densities, as measured by chronopotentiometry. The total current of the CO_2RR reaches 1.2 A (current density of 100 mA/cm^2) at a cell voltage of 3 V at room temperature, while increased temperature reduces the overpotential of the reaction to a cell voltage of 2.6 V at 50 °C and 2.4 V at 80 °C. A total current of 3 A (250 mA/cm^2) is achieved with a cell voltage of 3.63 V at room temperature, which is accessible with 2.97 V only at 80 °C. Fig. S7 reveals the CO volume fraction detected via gas chromatograph based on the CO_2 outlet flow. While maintaining a current density of 100 mA/cm^2, the CO_2RR produces similar CO volume fractions of 8 %–9 % at different temperatures. As the current density increases, the volume fraction of CO gradually grows to 20 %. The corresponding CO Faradaic efficiency (FE_{CO}) at various temperatures is presented in Fig. 3b, derived from the CO volume fraction. For the CO_2RR at room temperature, the FE_{CO} is 89.1 % at

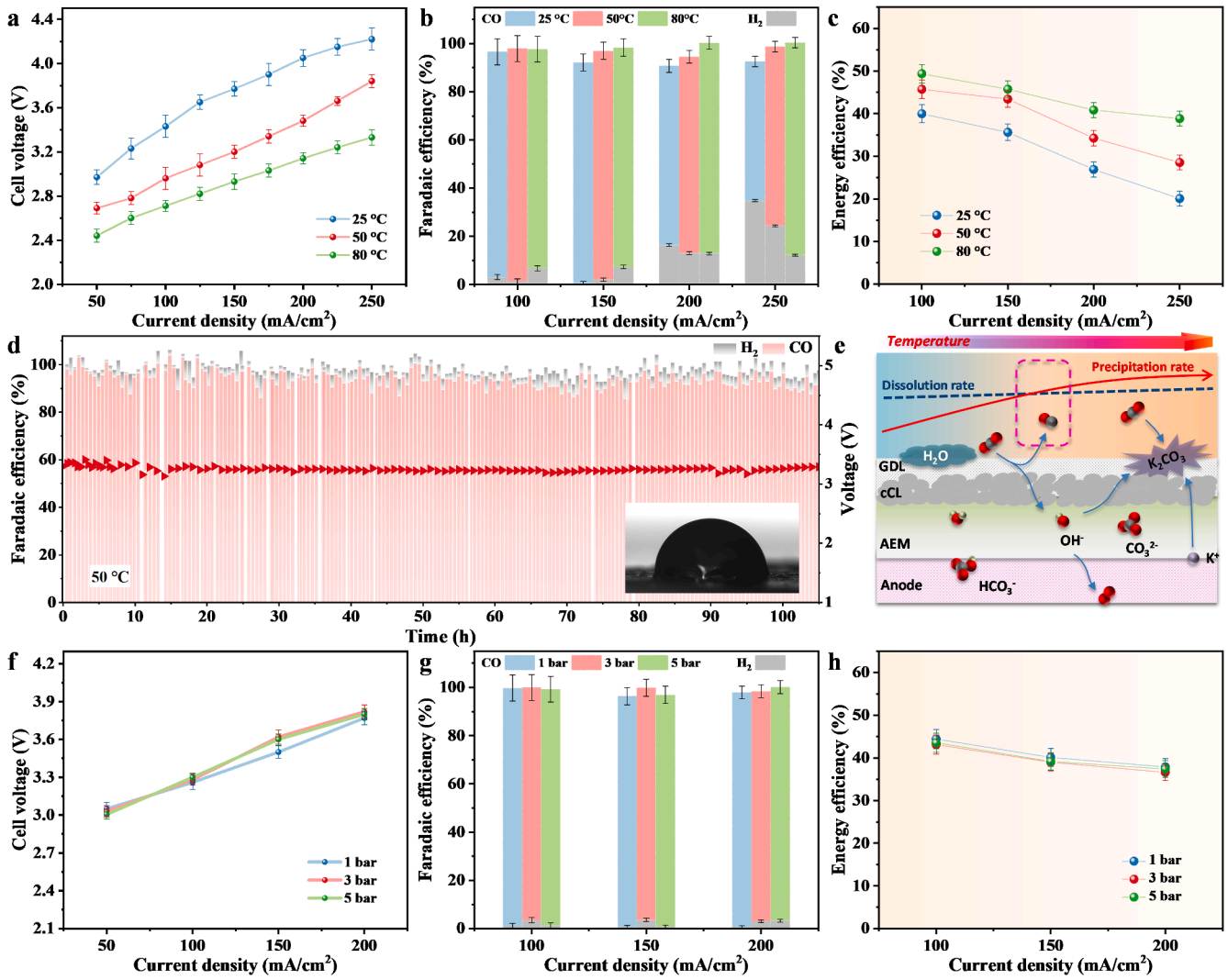

Fig. 4. CO_2RR performance with 0.1 M $KHCO_3$ anolyte in the modified zero-gap electrolyzer. (a) Polarization curves, (b) Faradaic efficiencies of CO and H_2 products, and (c) calculated energy efficiency at each current density under operation temperatures of 25 °C, 50 °C, and 80 °C. (d) Electrochemical stability test at a working current of 1.2 A under operation temperature of 50 °C. (e) Diagram of carbonate precipitation and dissolution. (f) Polarization curves, (g) Faradaic efficiencies, and (h) calculated energy efficiency at each current density.

a current density of 100 mA/cm^2. Despite the increased HER activity at higher current densities, FE_{CO} remains at 75.4 % even at a high current density of 250 mA/cm^2. At 50 °C, the CO_2RR maintains excellent CO selectivity across various current densities, achieving 93.0 %–94.0 % FE_{CO} at current densities of 100–200 mA/cm^2 and 87.1 % at 250 mA/cm^2. Even with the lowest cell voltage input at 80 °C, FE_{CO} values remain 85.7 %–88.0 % at current densities of 100–200 mA/cm^2 and 76.5 % at 250 mA/cm^2. In general, achieving a considerably high selectivity for target products at a lower voltage signifies an enhanced energy efficiency of the system (Fig. 3c). The catholyte-free operation and unobstructed mass transport result in a CO_2RR energy efficiency of 43.3 % at a current density of 100 mA/cm^2 and 33.3 % at 200 mA/cm^2 at room temperature. With the increased FE_{CO} at 50 °C, energy efficiency rises to 52.6 % at a current density of 100 mA/cm^2 and 44.3 % at 200 mA/cm^2. At 80 °C, the CO_2RR achieves comparable energy efficiencies of 52.5 % and 43.1 % with lower voltage. EIS was conducted to further analyze the effect of temperature on the CO_2RR in the zero-gap electrolyzer. Fig. 3d shows a slight decrease in ohmic resistance as the temperature increases, attributed to enhanced electronic conductivity and diffusion coefficients, which lead to higher reaction rates and CO selectivity. The consistent trend of higher operating temperatures yielding lower cell voltages benefits electrolyzers aiming for future commercial-scale current densities and energy efficiency [37]. Additionally, from an industrial viewpoint, waste heat from other chemical processes can sufficiently sustain CO_2 electrolyzer temperatures up to 80 °C [38].

During the CO_2RR process at a constant current of 1.2 A, Fig. 3e shows a gradual decrease in FE_{CO} across all tested temperatures while a noticeable increase in cell voltage only at room temperature. However, pressure fluctuation in the reactor halted the reactions after three hours, because solids formed at the cathode blocked the flow channels. SEM images of the tested Ag@Carbon electrodes reveal no obvious structural changes at the micron scale compared to the initial morphology (Fig. S8), while surface EDX spectroscopy (Table S1) identifies the presence of potassium on the electrode. This observation can be ascribed to electrolyte permeation driven by concentration and potential gradients, which further facilitates flooding and carbonate formation [39], thereby disturbing the gas–liquid equilibrium during electrolysis. Concurrently, the accumulated carbonate also imparts hydrophilic properties to the cathode surface [40,41]. This effect is manifested by the large decrease in water contact angles on the catalyst side of the Ag/C electrode to 63° (25 °C), 82° (50 °C), and 68° (80 °C) after 3 h (Fig. S9), indicating severe flooding and an increased prevalence of the HER as the experiment progressed.

Note that many chemical reactions using CO as a feedstock require elevated pressures [42]. As another strategy, CO_2 feed is pressurized to enhance the local concentration of CO_2 within the catalyst layer [43], which effectively shifts the onset potential positively on the LSV curves (Fig. S10). This adjustment is reconfirmed by the galvanostatic measurements, where the cell voltage decreases from 3.02 V at a current density of 100 mA/cm^2 under ambient conditions (Fig. 3a), to below 2.8 V when pressure is applied (Fig. 3f). Compared with CO_2RR at ambient pressure, the generated CO volume fractions also increased within a pressure range of 1 to 5 bar (Fig. S11). Pressurization increases the concentration of CO_2 reactants within the catalyst layer, further improving the single-pass conversion rate and the Faradaic efficiency of CO generation [44]. As shown in Fig. 3g, the total Faradaic efficiency of the product is close to 100 % at all tested current densities, which also demonstrates that the modified reactor with precision-engineered seal ensures stable operation and reliable measurements under demanding conditions. Adequate CO_2 supply is vital especially at high current density due to the substantial consumption required to sustain optimal reaction rates. Furthermore, Fig. 3h shows that the energy efficiency of the pressurized reaction ranges from 49.0 % to 51.7 % at a current density of 100 mA/cm^2 and from 31.2 % to 35.4 % at a higher current density of 250 mA/cm^2, attributed to improved Faradaic efficiency and reduced cell voltage. Therefore, pressurized CO_2 electrolysis may be a feasible method to directly provide CO product at the required pressure for downstream reproduction.

The foregoing analysis reveals that CO_2RR in the MEA-based reactor under alkaline conditions holds considerable potential for accelerating reaction rates. Elevating the temperature or pressure proves to be a wise strategy to enhance selectivity and the overall energy efficiency of the system. Nonetheless, it is noteworthy that CO_2 undergoes conversion to CO_3^{2-} in the alkaline environment, and the formation of these carbonates will obstruct CO_2 flow and diffusion, promoting hydrogen production [45,46]. Therefore, how to delay the production of carbonates or decompose carbonates over time while maintaining high current density without the system being destroyed is a key task for zero-gap electrolyzer systems.

3.3. Extended operation in neutral anolyte

Adopting a milder electrolyte, such as $KHCO_3$ solution with excellent buffering properties [47], appears to be a feasible approach to alleviating the problem of carbonate precipitation in the zero-gap electrolyzer. As shown from the LSV curves in Fig. S12, the AEM-MEA system with 0.1 M $KHCO_3$ anolyte demonstrates an enhanced reaction rate in elevated temperature environments, with a current from 2.2 A (25 °C) to 3.7 A (80 °C) at the same cell voltage of 4 V. The higher cell voltage in this case, compared to alkaline electrolytes, is due to the lower ion conductivity of HCO_3^- than OH^- and diminished reaction kinetics in a microenvironment with lower cation concentration and pH [48,49]. And the electrolyzer operated at a current density of 200 mA/cm^2 comes with corresponding voltages of 4.05 V, 3.48 V, and 3.14 V under operation temperatures of 25 °C, 50 °C, and 80 °C (Fig. 4a), respectively, which again underscores the temperature-dependent characteristics of the CO_2RR process. Fig. S13 highlights the direct correlation between current density and CO production, with a positive increase in the volume fraction ratio of CO as the operating current density rises. Fig. 4b reveals that FE_{CO} declines from approximately 93.5 % to 57.8 % at room temperature along with an increase of the working current density from 100 to 250 mA/cm^2. Although a slightly increased trend in HER is observed at large current densities at elevated temperatures, the MEA still maintained 88.2 % FE_{CO} at a current density of 250 mA/cm^2 at 80 °C. Fig. 4c shows that the corresponding energy efficiency increases at elevated temperatures for each given current density. Specifically, the energy efficiency of this MEA system at 80 °C approaches 49.4 % at a current density of 100 mA/cm^2 and still exceeds 40.8 % at 200 mA/cm^2. When the higher operating temperature appropriately offsets the heat requirement for CO_2-to-CO conversion, the demand for electrical energy decreases proportionally [50].

To affirm the stability of neutral CO_2RR in the zero-gap electrolyzer, life tests were conducted at a current density of 100 mA/cm^2 (total current 1.2 A) with 0.1 M $KHCO_3$ anolyte cycling. Over a 10-hour operation at room temperature, the required voltage increased progressively while the CO Faradaic efficiency declined modestly, as depicted in Fig. S14a. At an operating temperature of 80 °C, the voltage stabilized at 2.9 V with the FE_{CO} fluctuating around 90 % within 8 h (Fig. S14b). Both experiments were terminated after it was discovered that the pressure difference inside the reactor was increasing. More observations indicated that cathode GDL was flooded at room temperature after 10 h, whereas accumulated carbonate filled the microchannels after 8 h at 80 °C. However, it is worth noting that the system maintained a stable voltage of 3.2 V for over 100 h at 50 °C, with a CO Faradaic efficiency exceeding 90 % (Fig. 4d). Here, the inserted water contact angle image of the used Ag@Carbon electrode confirms the retention of hydrophobicity after service, and the SEM image (Fig. S15) shows no significant structural changes of the catalyst layer. Again, small amounts of potassium are detected on the cathode GDL surface, as evidenced by EDX analysis in Table S2. Thus, the temperature-dependent strategy is responsible for the high efficiency and extended operation lifetime. Fig. 4e illustrates a schematic depiction of the dynamic process within a zero-gap electrolytic cell, highlighting the impact of temperature on both dissolution and precipitation rates. In the process of electrolysis, potassium ions electrically migrate the cathode and interact with the alkaline microenvironment there, which facilitates carbonate compound formation [20]. Water vapor from the humidified CO_2 gas stream and water transported from the anode to the cathode through the membrane participate as reactants in the CO_2RR [51]. Some of this water accumulates within the cathode channels at room temperature, which dissolves the formed carbonates but can also cause flooding problems over time. As temperature increases, both the electroreduction reaction and carbonate precipitation accelerate as well as water evaporation losses on the cathode. This results in less available liquid water and more carbonate accumulation when the reactor is overheated. At the optimal temperature, an equilibrium between carbonate production and dissolution can be established, where the strategic mass and heat transfer dynamic balance enables the advanced efficiency and long-term stability of the system. Thus, fine-tuning the temperature to manage the solid/gas/liquid microenvironment within the catalyst layer is essential for durable, efficient, and stable CO_2 electrolysis.

Besides, LSV curves in the neutral electrolyte also admit that increased pressure enhances the overall reaction rate compared to atmospheric pressure, as shown in Fig. S16. There is no wide difference in the CO_2RR reaction rate for pressure changes in the range of 1 to 5 bar in Fig. 4f, with a close to full score of FE_{CO} and a clear suppression of the HER as depicted in Fig. 4g, particularly evident under high current conditions. The energy efficiency of pressurized CO_2RR, highlighted in Fig. 4h, is attributable to improvements in Faradaic efficiency and reduced cell voltage. This configuration delivers sustained energy efficiencies from 43.1 % at a current of 1.2 A to 37.9 % at 2.4 A, compared to 37 % and 26 % at room temperature and atmospheric pressure. These interesting findings suggest that the approach of directly introducing pressurized CO_2 gas into the cathode effectively augments the local concentration of reactants to occupy a greater number of reaction sites and expedite CO desorption. Experiments have validated that the structured deployment of zero-gap electrolyzers combined with a synergistically engineered microenvironment can stimulate CO_2RR performance. Increasing the operating temperature and pressure can significantly accelerate the reaction kinetics and mass transport, thereby improving the energy efficiency of both alkaline and neutral electrolyte systems.

The influence of temperature on the activation energy (E_{act}) for CO_2-to-CO conversion in both electrolytes was quantitatively investigated,

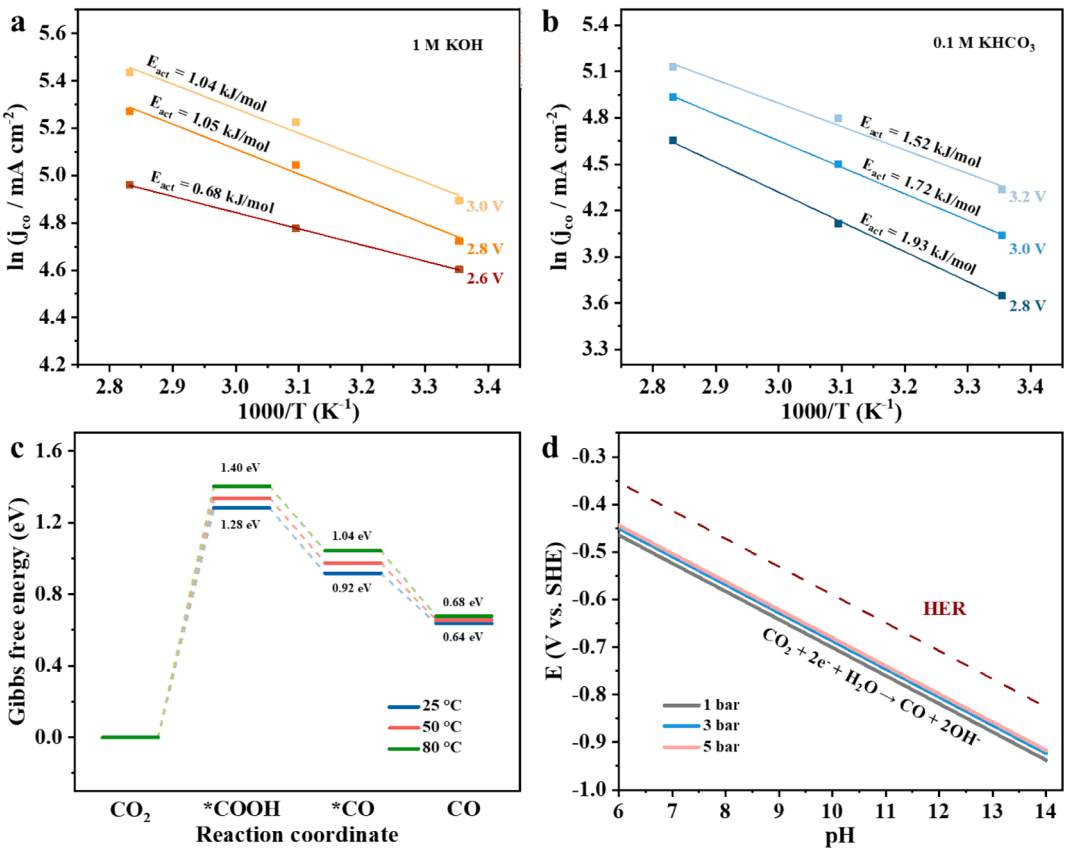

Fig. 5. Activation energy for CO_2 to CO in (a) alkaline and (b) neutral anolyte system. (c) Calculated free-energy diagram over Ag catalyst with different operation temperatures. (d) Effect of pressure on Pourbaix diagram for the electroreduction of CO_2 to CO.

which was achieved by plotting the linear fit of the natural logarithm of the CO partial current density against the inverse of temperature, following the Arrhenius equation over the temperature range of 298 K to 353 K [52,53]. Across the applied voltage conditions, the alkaline system (Fig. 5a) exhibited consistently lower E_{act} values compared to the neutral system (Fig. 5b), demonstrating superior CO production efficiency under alkaline conditions. Furthermore, density functional theory (DFT) calculations (Fig. S17) revealed that increasing the temperature on the Ag catalyst surface elevates the Gibbs free energy associated with the formation of *COOH intermediates but promotes the desorption of CO products, as depicted in Fig. 5c. Additionally, the effect of pressure was clarified in Fig. 5d by Pourbaix diagram derived from the Nernst equation [54]. With increasing pressure, the Pourbaix line for the CO_2-to-CO reaction shifts upward, indicating a slight reduction in the overpotential. Moreover, as per Le Chatelier's principle [44], higher pressure and increased reactant concentrations enhance both the reaction rate and the conversion efficiency of CO_2. Table S3 lists some studies reporting the performance metrics of CO_2-to-CO conversion in MEA-based electrolyzers. This compilation highlights that the modified electrolyzer in this study achieves a combination of high current density and low operating voltage over a relatively large electrode area with controllable temperature and pressure, thereby delivering high energy efficiency and long-term operation stability, and these attributes remain key breakthrough points for future developments in this field.

4. Conclusion

In addressing the challenges of scalability and feasibility of the CO_2 electroreduction system, this work discovered a route towards enhanced energy efficiency and prolonged operational lifetime. This work found that the demands for low voltage and high current density in practical scenarios could be achieved by adjusting reactor temperature and pressure, which in turn increased reaction rate and efficiency. Furthermore, the water vapor in humidified CO_2 helped to mitigate the carbonate precipitation issue at the cathode in a neutral anolyte. These adjustments have demonstrated a 10 %–20 % improvement in the energy conversion efficiency of the MEA electrolyzer system compared to ambient environment conditions. The integration of engineering strategies and the microenvironmental adjustment in a zero-gap MEA electrolyzer establishes a balance among electrochemical parameters, enhancing the efficiency and practicality of CO_2RR, which is expected to provide valuable insights for future large-scale CO_2 reduction applications.

CRediT authorship contribution statement

Siyu Zhong: Writing – original draft, Validation, Investigation, Formal analysis, Data curation, Conceptualization. **Pengfei Sui:** Investigation, Methodology, Software, Validation, Writing – review & editing. **Peter Holtappels:** Writing – review & editing, Supervision. **Alexander Navarrete:** Writing – review & editing, Supervision. **Fengwang Li:** Writing – review & editing. **Roland Dittmeyer:** Writing – review & editing, Supervision, Funding acquisition.

Declaration of competing interest

The authors declare that they have no known competing financial interests or personal relationships that could have appeared to influence the work reported in this paper.

Acknowledgments

We gratefully acknowledge the financial support from the Helmholtz Association of German Research Centers within the Helmholtz-Program: MTET Materials and Technologies for the Energy Transition (Topic 3: Chemical Energy Carriers), and HI-CAM II, Cluster I, Net Zero 2050. S.Z. thanks Mr. Wenwu Yang and Dr. Michael Zimmermann for the SEM and EDS characterization, Dr. Peter G. Weidler for the XRD measurement, and Mr. Sida Liu for the water contact angle test. F.L. is grateful for the support from the ARC Centre of Excellence for Green Electrochemical Transformation of Carbon Dioxide (CE230100017) funded by the Australian Government. S.Z. thanks the Karlsruhe House for Young Scientists (KHYS) for a research travel grant.

Appendix A. Supplementary data

Supplementary data to this article can be found online at https://doi.org/10.1016/j.cej.2025.161119.

Data availability

Data will be made available on request.

References

[1] Z. Xie, E. Huang, S. Garg, S. Hwang, P. Liu, J.G. Chen, CO_2 fixation into carbon nanofibres using electrochemical–thermochemical tandem catalysis, Nat. Catal. 7 (2024) 98–109.
[2] K. Qi, Y. Zhang, N. Onofrio, E. Petit, X. Cui, J. Ma, J. Fan, H. Wu, W. Wang, J. Li, J. Liu, Y. Zhang, Y. Wang, G. Jia, J. Wu, L. Lajaunie, C. Salameh, D. Voiry, Unlocking direct CO_2 electrolysis to C3 products via electrolyte supersaturation, Nat. Catal. 6 (2023) 319–331.
[3] Y. Liang, F. Li, R.K. Miao, S. Hu, W. Ni, S. Zhang, Y. Liu, Y. Bai, H. Wan, P. Ou, X.-Y. Li, N. Wang, S. Park, F. Li, J. Zeng, D. Sinton, E.H. Sargent, Efficient ethylene electrosynthesis through C–O cleavage promoted by water dissociation, Nat. Synth. 3 (2024) 1104–1112.
[4] X. Wang, Z. Wang, T.T. Zhuang, C.T. Dinh, J. Li, D.H. Nam, F. Li, C.W. Huang, C. S. Tan, Z. Chen, M. Chi, C.M. Gabardo, A. Seifitokaldani, P. Todorovic, A. Proppe, Y. Pang, A.R. Kirmani, Y. Wang, A.H. Ip, L.J. Richter, B. Scheffel, A. Xu, S.C. Lo, S. O. Kelley, D. Sinton, E.H. Sargent, Efficient upgrading of CO to C3 fuel using asymmetric C-C coupling active sites, Nat. Commun. 10 (2019) 5186.
[5] D. Dhamo, J. Kühn, S. Lüttin, M. Rubin, R. Dittmeyer, Coupling the high-temperature Fischer-Tropsch synthesis and the skeletal isomerization reaction at optimal operation conditions in the Power-to-Fuels process route for the production of sustainable aviation gasoline, Sustain. Energy Fuels 8 (2024) 2094–2103.
[6] D. Segets, C. Andronescu, U.P. Apfel, Accelerating CO_2 electrochemical conversion towards industrial implementation, Nat. Commun. 14 (2023) 7950.
[7] W. Lai, Y. Qiao, J. Zhang, Z. Lin, H. Huang, Design strategies for markedly enhancing energy efficiency in the electrocatalytic CO_2 reduction reaction, Energ. Environ. Sci. 15 (2022) 3603–3629.
[8] H. Zhang, J. Gao, D. Raciti, A.S. Hall, Promoting Cu-catalysed CO_2 electroreduction to multicarbon products by tuning the activity of H_2O, Nat. Catal. 6 (2023) 807–817.
[9] M. Esmaeilirad, Z. Jiang, A.M. Harzandi, A. Kondori, M. Tamadoni Saray, C. U. Segre, R. Shahbazian-Yassar, A.M. Rappe, M. Asadi, Imidazolium-functionalized Mo_3P nanoparticles with an ionomer coating for electrocatalytic reduction of CO_2 to propane, Nat. Energy 8 (2023) 891–900.
[10] Y. Yang, C. Zhang, C. Zhang, Y. Shi, J. Li, B. Johannessen, Y. Liang, S. Zhang, Q. Song, H. Zhang, J. Huang, J. Ke, L. Zhang, Q. Song, J. Zeng, Y. Zhang, Z. Geng, P.S. Wang, Z. Wang, J. Zeng, F. Li, Ligand-tuning copper in coordination polymers for efficient electrochemical C-C coupling, Nat. Commun. 15 (2024) 6316.
[11] C. Xia, P. Zhu, Q. Jiang, Y. Pan, W. Liang, E. Stavitski, H.N. Alshareef, H. Wang, Continuous production of pure liquid fuel solutions via electrocatalytic CO_2 reduction using solid-electrolyte devices, Nat. Energy 4 (2019) 776–785.
[12] A. Ozden, F.P.G. De Arquer, J.E. Huang, J. Wicks, J. Sisler, R.K. Miao, C.P. O'Brien, G. Lee, X. Wang, A.H. Ip, E.H. Sargent, D. Sinton, Carbon-efficient carbon dioxide electrolysers, Nat. Sustain. 5 (2022) 563–573.
[13] B.S. Crandall, B.H. Ko, S. Overa, L. Cherniack, A. Lee, I. Minnie, F. Jiao, Kilowatt-scale tandem CO_2 electrolysis for enhanced acetate and ethylene production, Nat. Chem. Eng. 1 (2024) 421–429.
[14] L. Weng, A.T. Bell, A.Z. Weber, Towards membrane-electrode assembly systems for CO_2 reduction: a modeling study, Energ. Environ. Sci. 12 (2019) 1950–1968.
[15] L. Ge, H. Rabiee, M. Li, S. Subramanian, Y. Zheng, J.H. Lee, T. Burdyny, H. Wang, Electrochemical CO_2 reduction in membrane-electrode assemblies, Chem 8 (2022) 663–692.
[16] S. Brückner, Q. Feng, W. Ju, D. Galliani, A. Testolin, M. Klingenhof, S. Ott, P. Strasser, Design and diagnosis of high-performance CO_2-to-CO electrolyzer cells, Nat. Chem. Eng. 1 (2024) 229–239.
[17] E.K. Volk, M.E. Kreider, S. Kwon, S.M. Alia, Recent progress in understanding the catalyst layer in anion exchange membrane electrolyzers – durability, utilization, and integration, EES Catal. 2 (2024) 109–137.
[18] X. Zhao, H. Xie, B. Deng, L. Wang, Y. Li, F. Dong, Enhanced CO_2 reduction with hydrophobic cationic-ionomer layer-modified zero-gap MEA in acidic electrolyte, Chem. Commun. 60 (2024) 542–545.
[19] F.P. Garcia de Arquer, C.T. Dinh, A. Ozden, J. Wicks, C. McCallum, A.R. Kirmani, D.H. Nam, C. Gabardo, A. Seifitokaldani, X. Wang, Y.C. Li, F. Li, J. Edwards, L. J. Richter, S.J. Thorpe, D. Sinton, E.H. Sargent, CO_2 electrolysis to multicarbon products at activities greater than 1 A cm^{-2}, Science 367 (2020) 661–666.
[20] M. Sassenburg, M. Kelly, S. Subramanian, W.A. Smith, T. Burdyny, Zero-gap electrochemical CO_2 reduction cells: challenges and operational strategies for prevention of salt precipitation, ACS Energy Lett. 8 (2023) 321–331.
[21] D.A. Salvatore, C.M. Gabardo, A. Reyes, C.P. O'Brien, S. Holdcroft, P. Pintauro, B. Bahar, M. Hickner, C. Bae, D. Sinton, E.H. Sargent, C.P. Berlinguette, Designing anion exchange membranes for CO_2 electrolysers, Nat. Energy 6 (2021) 339–348.
[22] C. Zhu, G. Wu, A. Chen, G. Feng, X. Dong, G. Li, S. Li, Y. Song, W. Wei, W. Chen, Selective CO_2 electroreduction to multicarbon products exceeding 2 A cm^{-2} in strong acids via a hollow-fiber Cu penetration electrode, Energ. Environ. Sci. 17 (2024) 510–517.
[23] X. She, L. Zhai, Y. Wang, P. Xiong, M.-M.-J. Li, T.-S. Wu, M.C. Wong, X. Guo, Z. Xu, H. Li, H. Xu, Y. Zhu, S.C.E. Tsang, S.P. Lau, Pure-water-fed, electrocatalytic CO_2 reduction to ethylene beyond 1,000 h stability at 10 A, Nat. Energy 9 (2024) 81–91.
[24] Z. Yin, H. Peng, X. Wei, H. Zhou, J. Gong, M. Huai, L. Xiao, G. Wang, J. Lu, L. Zhuang, An alkaline polymer electrolyte CO_2 electrolyzer operated with pure water, Energ. Environ. Sci. 12 (2019) 2455–2462.
[25] G.X. Liu, D. McLaughlin, S. Thiele, C. Van Pham, Correlating catalyst ink design and catalyst layer fabrication with electrochemical CO_2 reduction performance, Chem. Eng. J. 460 (2023) 141757.
[26] C.P. O'Brien, R.K. Miao, A. Shayesteh Zeraati, G. Lee, E.H. Sargent, D. Sinton, CO_2 electrolyzers, Chem. Rev. 124 (2024) 3648–3693.
[27] T. Haas, R. Krause, R. Weber, M. Demler, G. Schmid, Technical photosynthesis involving CO_2 electrolysis and fermentation, Nat. Catal. 1 (2018) 32–39.
[28] A.J. Martín, G.O. Larrazábal, J. Pérez-Ramírez, Towards sustainable fuels and chemicals through the electrochemical reduction of CO_2: lessons from water electrolysis, Green Chem. 17 (2015) 5114–5130.
[29] Y. Zhong, X. Kong, Z. Song, Y. Liu, L. Peng, L. Zhang, X. Luo, J. Zeng, Z. Geng, Adjusting local CO confinement in porous-shell Ag@Cu catalysts for enhancing C-C coupling toward CO_2 eletroreduction, Nano Lett. 22 (2022) 2554–2560.
[30] Y. Ma, W. Niu, W. Shi, X. Huang, Y. Liu, J. Chen, L. Xue, B. Zhang, Amorphous carbon coating enhances activity of high rate CO_2 electroreduction to CO, J. Mater. Chem. A 11 (2023) 12114–12120.
[31] Y.C. Tan, K.B. Lee, H. Song, J. Oh, Modulating local CO_2 concentration as a general strategy for enhancing C-C coupling in CO_2 electroreduction, Joule 4 (2020) 1104–1120.
[32] H. Rabiee, L. Ge, X.Q. Zhang, S.H. Hu, M.R. Li, Z.G. Yuan, Gas diffusion electrodes (GDEs) for electrochemical reduction of carbon dioxide, carbon monoxide, and dinitrogen to value-added products: a review, Energ. Environ. Sci. 14 (2021) 1959–2008.
[33] R. Shi, J. Guo, X. Zhang, G.I.N. Waterhouse, Z. Han, Y. Zhao, L. Shang, C. Zhou, L. Jiang, T. Zhang, Efficient wettability-controlled electroreduction of CO_2 to CO at Au/C interfaces, Nat. Commun. 11 (2020) 3028.
[34] Z. Xing, L. Hu, D.S. Ripatti, X. Hu, X. Feng, Enhancing carbon dioxide gas-diffusion electrolysis by creating a hydrophobic catalyst microenvironment, Nat. Commun. 12 (2021) 136.
[35] W. Lee, Y.E. Kim, M.H. Youn, S.K. Jeong, K.T. Park, Catholyte-free electrocatalytic CO_2 reduction to formate, Angew. Chem. Int. Ed. Engl. 57 (2018) 6883–6887.
[36] M.G. Kibria, J.P. Edwards, C.M. Gabardo, C.T. Dinh, A. Seifitokaldani, D. Sinton, E. H. Sargent, Electrochemical CO_2 reduction into chemical feedstocks: from mechanistic electrocatalysis models to system design, Adv. Mater. 31 (2019) 1807166.
[37] H.W. Shafaque, J.K. Lee, K. Krause, C. Lee, K.F. Fahy, P. Shrestha, M. Balakrishnan, A. Bazylak, Temperature enhances the ohmic and mass transport behaviour in membrane electrode assembly carbon dioxide electrolyzers, Energ Convers Manage 243 (2021) 114302.
[38] S. Garg, Q. Xu, A.B. Moss, M. Mirolo, W. Deng, I. Chorkendorff, J. Drnec, B. Seger, How alkali cations affect salt precipitation and CO_2 electrolysis performance in membrane electrode assembly electrolyzers, Energ. Environ. Sci. 16 (2023) 1631–1643.
[39] M. Ramdin, O.A. Moultos, L.J.P. van den Broeke, P. Gonugunta, P. Taheri, T.J. H. Vlugt, Carbonation in low-temperature CO_2 electrolyzers: causes, consequences, and solutions, Ind. Eng. Chem. Res. 62 (2023) 6843–6864.
[40] A. Reyes, R.P. Jansonius, B.A.W. Mowbray, Y. Cao, D.G. Wheeler, J. Chau, D. J. Dvorak, C.P. Berlinguette, Managing hydration at the cathode enables efficient CO_2 electrolysis at commercially relevant current densities, ACS Energy Lett. 5 (2020) 1612–1618.
[41] K. Liu, W.A. Smith, T. Burdyny, Introductory guide to assembling and operating gas diffusion electrodes for electrochemical CO_2 reduction, ACS Energy Lett. 4 (2019) 639–643.
[42] S. Lyu, L. Wang, Z. Li, S. Yin, J. Chen, Y. Zhang, J. Li, Y. Wang, Stabilization of epsilon-iron carbide as high-temperature catalyst under realistic Fischer-Tropsch synthesis conditions, Nat. Commun. 11 (2020) 6219.

[43] L. Huang, G. Gao, C. Yang, X.Y. Li, R.K. Miao, Y. Xue, K. Xie, P. Ou, C.T. Yavuz, Y. Han, G. Magnotti, D. Sinton, E.H. Sargent, X. Lu, Pressure dependence in aqueous-based electrochemical CO_2 reduction, Nat. Commun. 14 (2023) 2958.
[44] N.C. Kani, S. Olusegun, R. Chauhan, J.A. Gauthier, M.R. Singh, High-pressure electrochemistry: a new frontier in decarbonization, EES Catal. 2 (2024) 507–521.
[45] Y. Chen, X.Y. Li, Z. Chen, A. Ozden, J.E. Huang, P. Ou, J. Dong, J. Zhang, C. Tian, B.H. Lee, X. Wang, S. Liu, Q. Qu, S. Wang, Y. Xu, R.K. Miao, Y. Zhao, Y. Liu, C. Qiu, J. Abed, H. Liu, H. Shin, D. Wang, Y. Li, D. Sinton, E.H. Sargent, Efficient multicarbon formation in acidic CO_2 reduction via tandem electrocatalysis, Nat. Nanotechnol. 19 (2024) 311–318.
[46] C.T. Dinh, T. Burdyny, M.G. Kibria, A. Seifitokaldani, C.M. Gabardo, F.P. Garcia de Arquer, A. Kiani, J.P. Edwards, P. De Luna, O.S. Bushuyev, C. Zou, R. Quintero-Bermudez, Y. Pang, D. Sinton, E.H. Sargent, CO_2 electroreduction to ethylene via hydroxide-mediated copper catalysis at an abrupt interface, Science 360 (2018) 783–787.
[47] G. Wen, B. Ren, X. Wang, D. Luo, H. Dou, Y. Zheng, R. Gao, J. Gostick, A. Yu, Z. Chen, Continuous CO_2 electrolysis using a CO_2 exsolution-induced flow cell, Nat. Energy 7 (2022) 978–988.
[48] J. Disch, L. Bohn, L. Metzler, S. Vierrath, Strategies for the mitigation of salt precipitation in zero-gap CO_2 electrolyzers producing CO, J. Mater. Chem. A 11 (2023) 7344–7357.
[49] C.M. Gabardo, C.P. O'Brien, J.P. Edwards, C. McCallum, Y. Xu, C.T. Dinh, J. Li, E. H. Sargent, D. Sinton, Continuous carbon dioxide electroreduction to concentrated multi-carbon products using a membrane electrode assembly, Joule 3 (2019) 2777–2791.
[50] S.D. Ebbesen, S.H. Jensen, A. Hauch, M.B. Mogensen, High temperature electrolysis in alkaline cells, solid proton conducting cells, and solid oxide cells, Chem. Rev. 114 (2014) 10697–10734.
[51] D.G. Wheeler, B.A.W. Mowbray, A. Reyes, F. Habibzadeh, J.F. He, C. P. Berlinguette, Quantification of water transport in a CO_2 electrolyzer, Energ. Environ. Sci. 13 (2020) 5126–5134.
[52] D. Kim, W. Choi, H.W. Lee, S.Y. Lee, Y. Choi, D.K. Lee, W. Kim, J. Na, U. Lee, Y. J. Hwang, D.H. Won, Electrocatalytic reduction of low concentrations of CO_2 gas in a membrane electrode assembly electrolyzer, ACS Energy Lett. 6 (2021) 3488–3495.
[53] U.O. Nwabara, M.P. de Heer, E.R. Cofell, S. Verma, E. Negro, P.J.A. Kenis, Towards accelerated durability testing protocols for CO_2 electrolysis, J. Mater. Chem. A 8 (2020) 22557–22571.
[54] S. Verma, Y. Hamasaki, C. Kim, W. Huang, S. Lu, H.M. Jhong, A.A. Gewirth, T. Fujigaya, N. Nakashima, P.J.A. Kenis, Insights into the low overpotential electroreduction of CO_2 to CO on a supported gold catalyst in an alkaline flow electrolyzer, ACS Energy Lett. 3 (2017) 193–198.